Electronic Supplementary Information

Metal-Organic Frameworks (MOFs) Facilitated Highly Stretchable, and Fatigue-Resistant Ionogels for Recyclable Sensors

*Qunmeng Xia,[†] Weizheng Li,[†] Xiuyang Zou, Sijie Zheng, Ziyang Liu, Lingling Li and Feng Yan**

Jiangsu Engineering Laboratory of Novel Functional Polymeric Materials, Jiangsu Key Laboratory of Advanced Negative Carbon Technologies College of Chemistry, Chemical Engineering and Materials Science, Soochow University, Suzhou 215123, China.

E-mail: fyan@suda.edu.cn

[†]Authors with equal contributions.

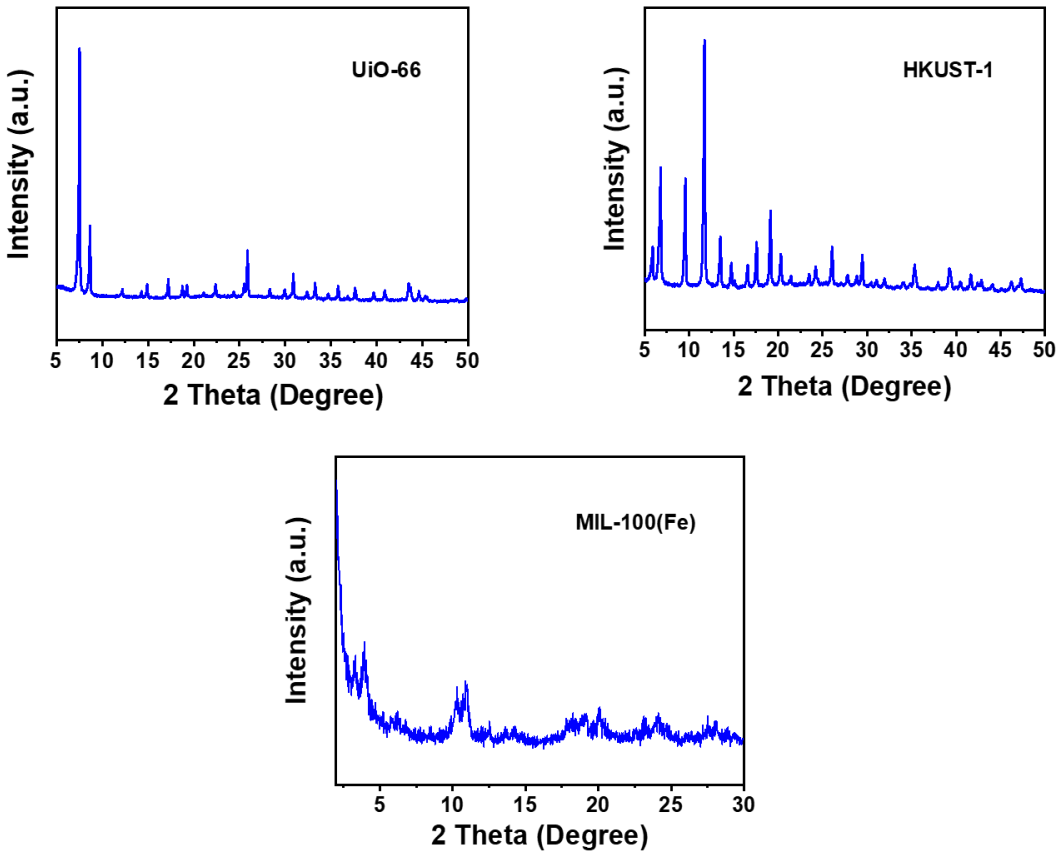

Figure S1. Powder X-ray diffraction (PXRD) patterns of three MOFs (UiO-66, HKUST-1, MIL-100(Fe)). Consistent with the XRD in the literature.[S1-S3]

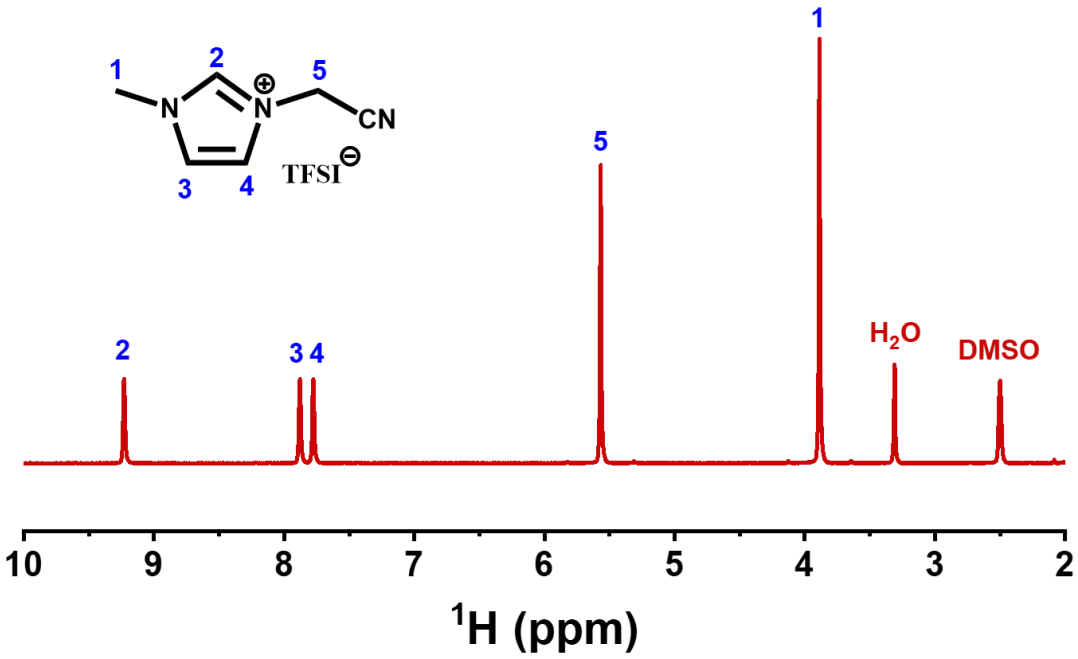

Figure S2. ^{1}H NMR spectroscopy of 1-cyanomethyl-3-methylimidazolium bis[(trifluoromethyl)sulfonyl]imide ([CMMIM]TFSI).

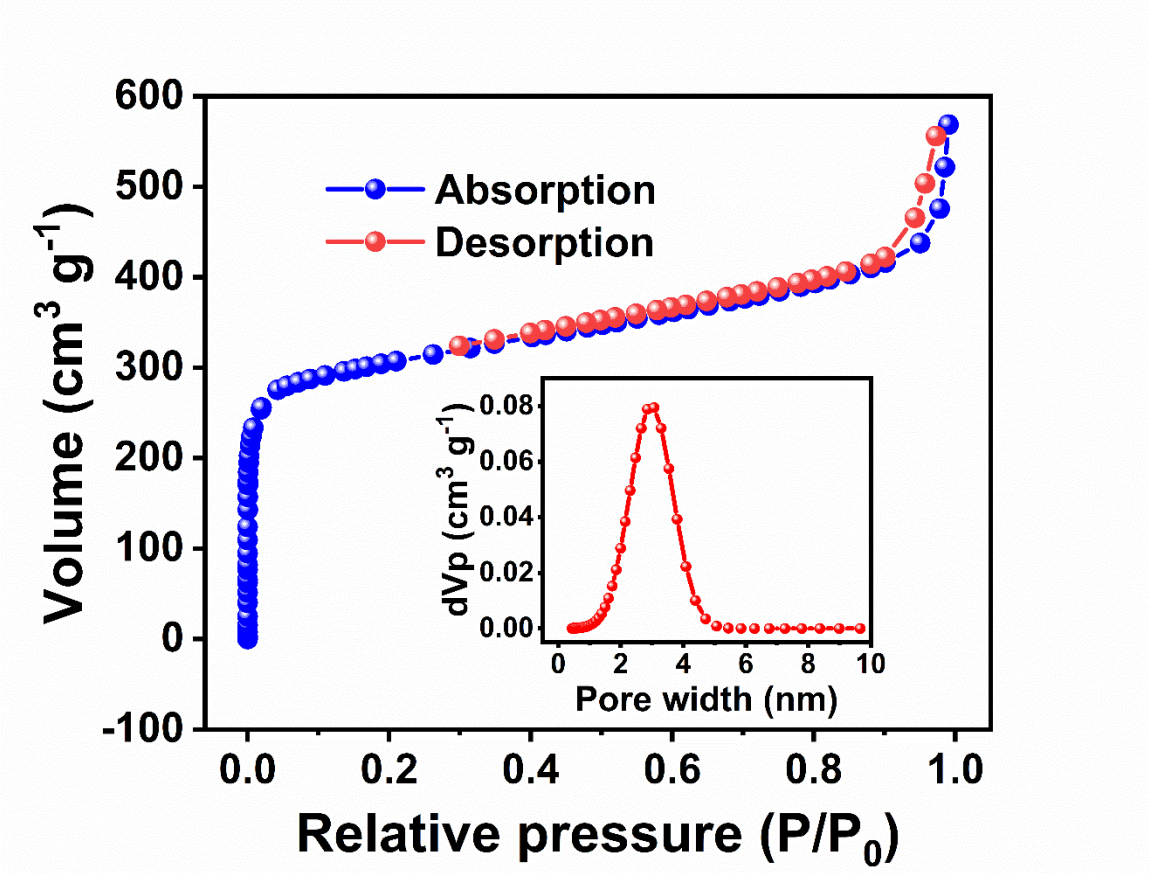

Figure S3. Nitrogen adsorption isotherms of UiO-66, and pore-size distributions (inset).

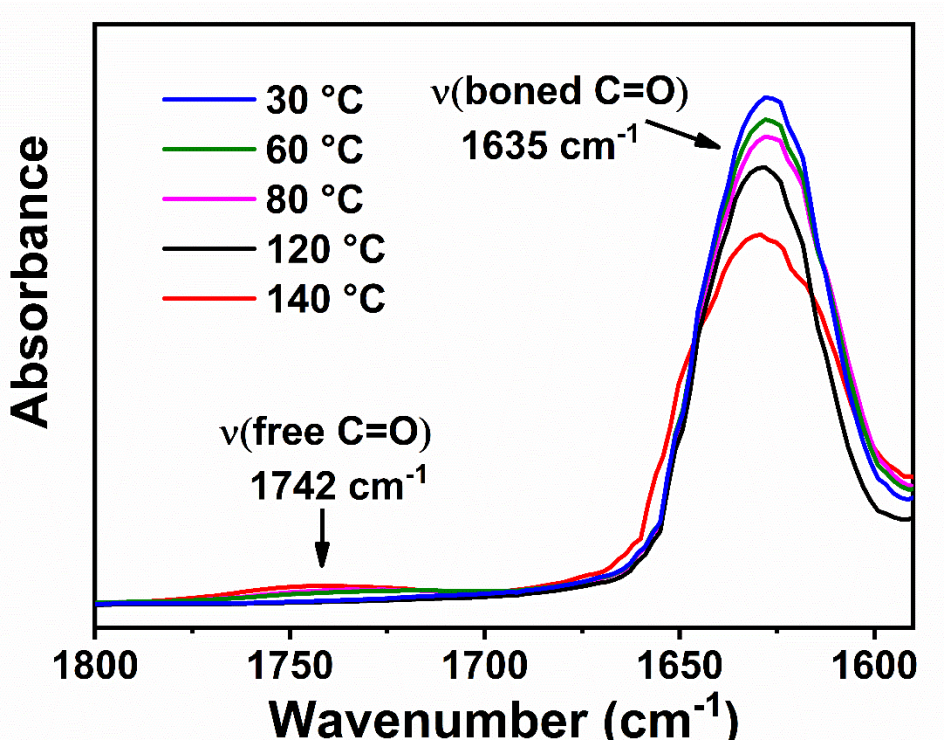

Figure S4. FT-IR spectra of UiO-66-ionogel under different temperature.

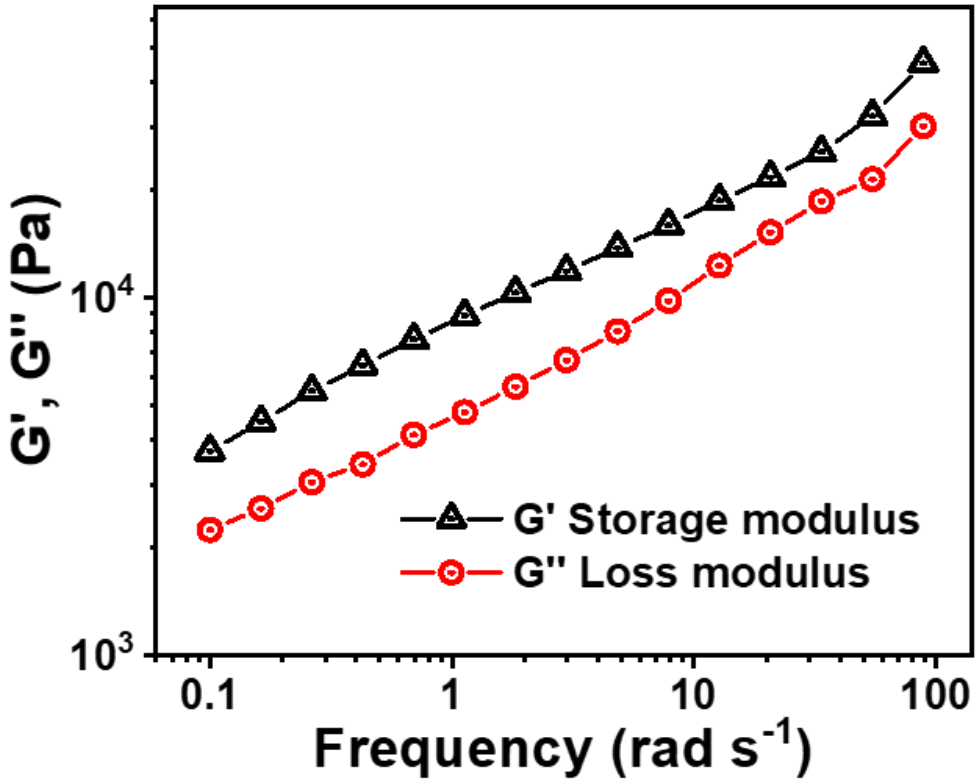

Figure S5. Storage modulus G', and loss modulus G'' of UiO-66-ionogel (IL: 90 wt%, UiO-66: 0.5 wt%) on frequency sweep at 25 ℃.

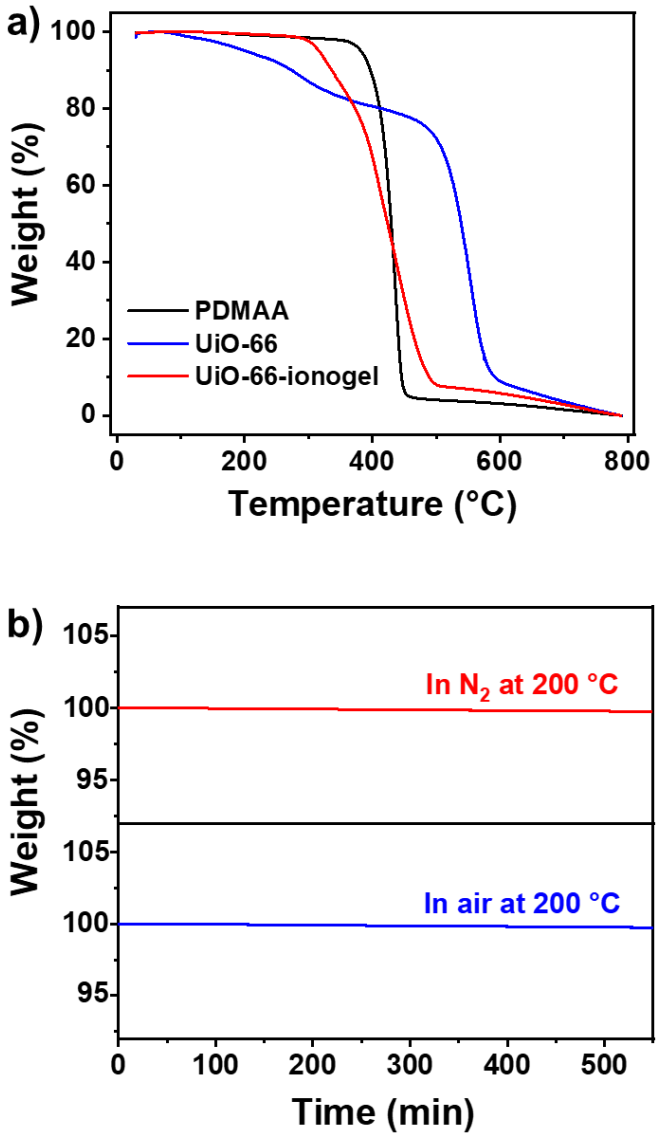

Figure S6. (a) Thermal decomposition curves of the PDMAA, UiO-66, and UiO-66-ionogel from 30 ℃ to 800 ℃. PDMAA, UiO-66, and UiO-66-ionogel exhibited T_d (T_d: the onset decomposition temperature corresponding to the temperature at which the percent weight loss is approximately 5%) at 364 ℃, 93 ℃, and 295 ℃, respectively. (b) Long-term durability of UiO-66-ionogel in N_2 and air at 200 ℃. The test was performed at a heating rate of 10 ℃ min^{-1} under flowing N_2 and air, respectively.

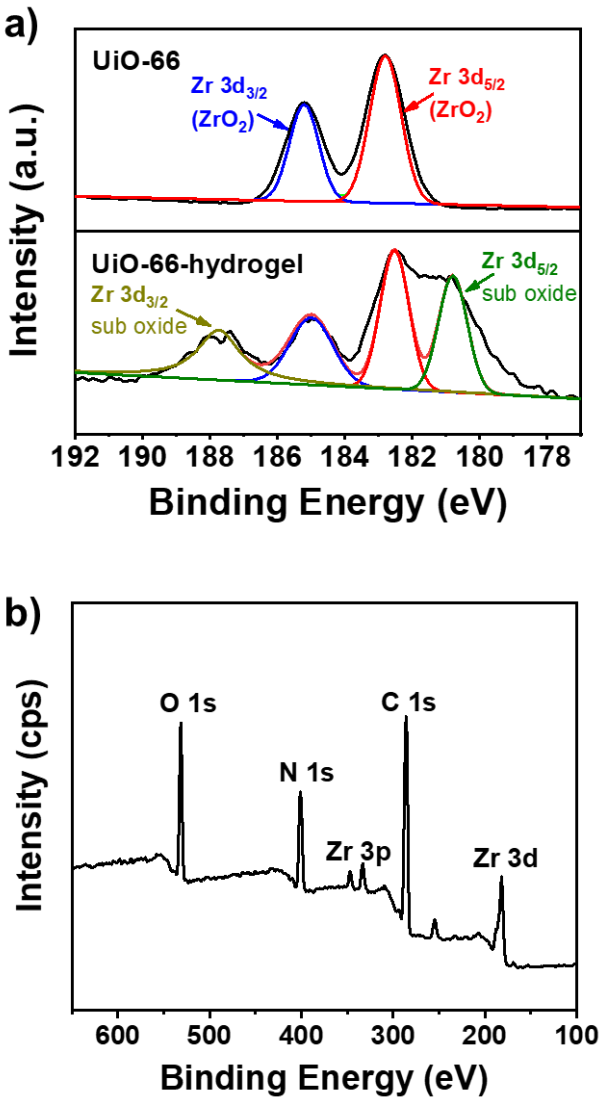

Figure S7. (a) Zr 3d results of X-ray photoelectron spectroscopy (XPS) spectrum for UiO-66 and UiO-66-polymer. The Zr of UiO-66 will be separated into two $3d_{3/2}$ (185.2 eV) and $3d_{5/2}$ (182.7 eV) due to the electron spin. However, because the cyano group has a strong coordination effect, it will compete with the ligand on UiO-66 for coordination, so that part of the Zr is coordinated with the cyano group, and the XPS energy spectrum shows two sub oxide peaks $3d_{3/2}$ (187.7 eV) and $3d_{5/2}$ (180.8 eV). The results show that part of the Zr in UiO-66 is coordinated with the cyano group to form a new coordination bond. (b) XPS spectrum of UiO-66-polymer.

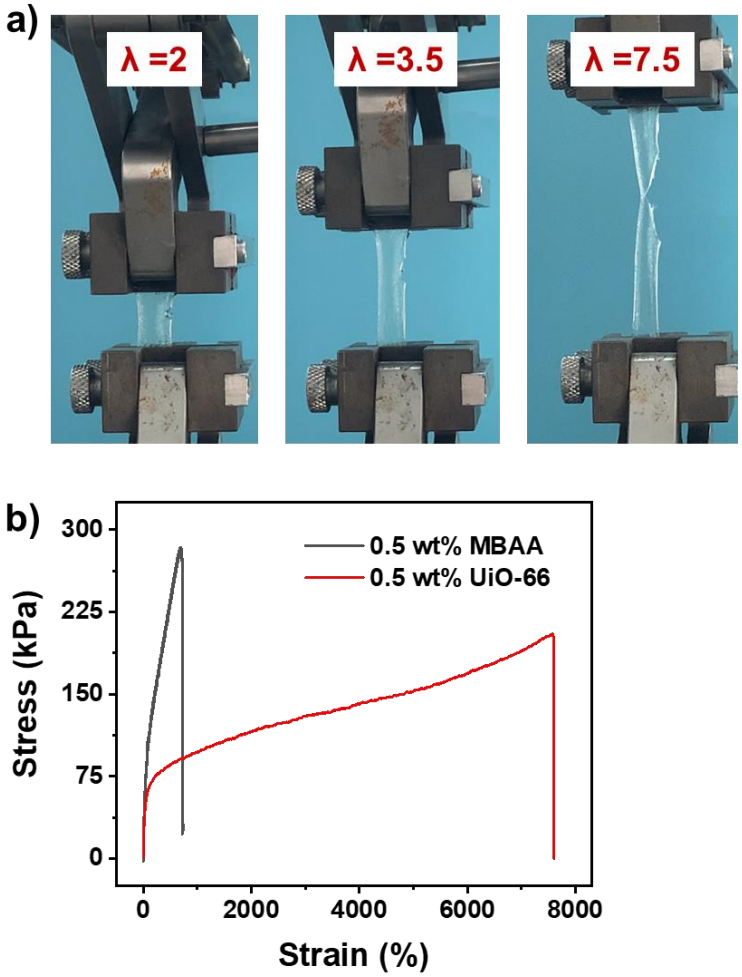

Figure S8. (a) Monotonic tensile photographs of notched ionogel containing 0.5 wt% chemical crosslinking agent (MBAA). (b) Comparison of tear resistance between UiO-66 and chemical crosslinker (MBAA) (stretching rate: 50 mm min^{-1}).

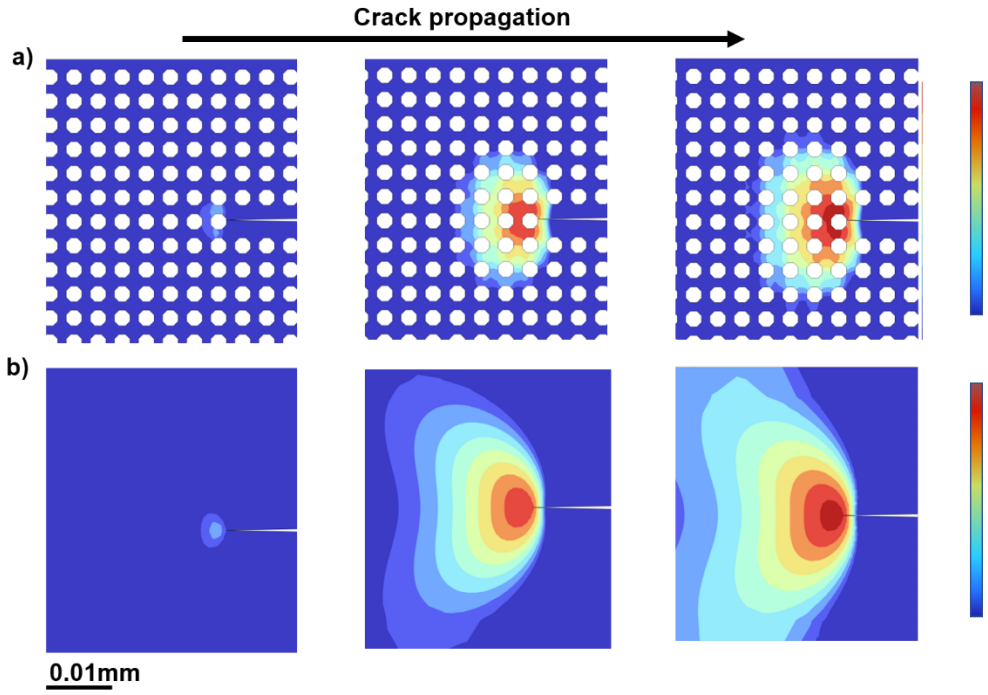

Figure S9. Finite element simulations of the crack damage area inside (a)UiO-66-ionogel and (b) ionogel containing chemical crosslinking agent (MBAA).

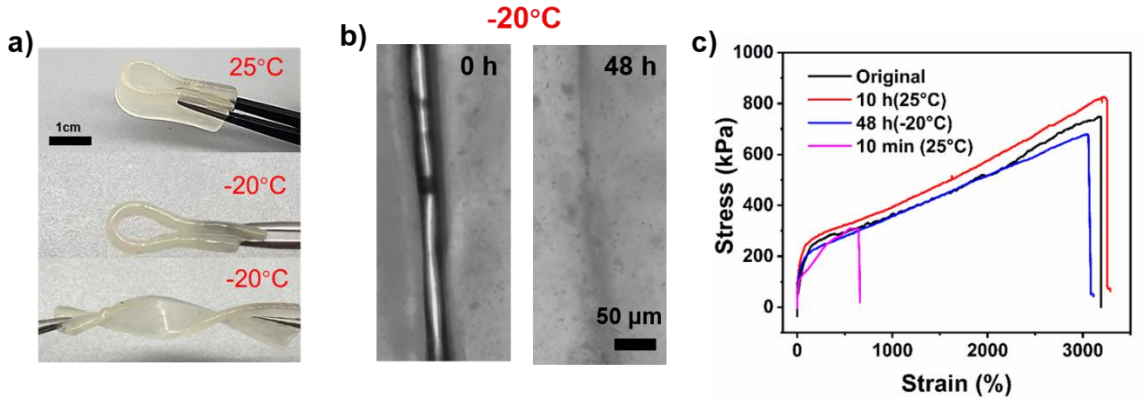

Figure S10. (a) Photographs of UiO-66-ionogel being bent and twisted at 25 and −20 °C. (b) Images of completely severed specimens were obtained using an optical microscope at different self-healing time at -20 ℃. (c) Monotonic variations in the tensile stress-strain curves of UiO-66-ionogel after self-healing.

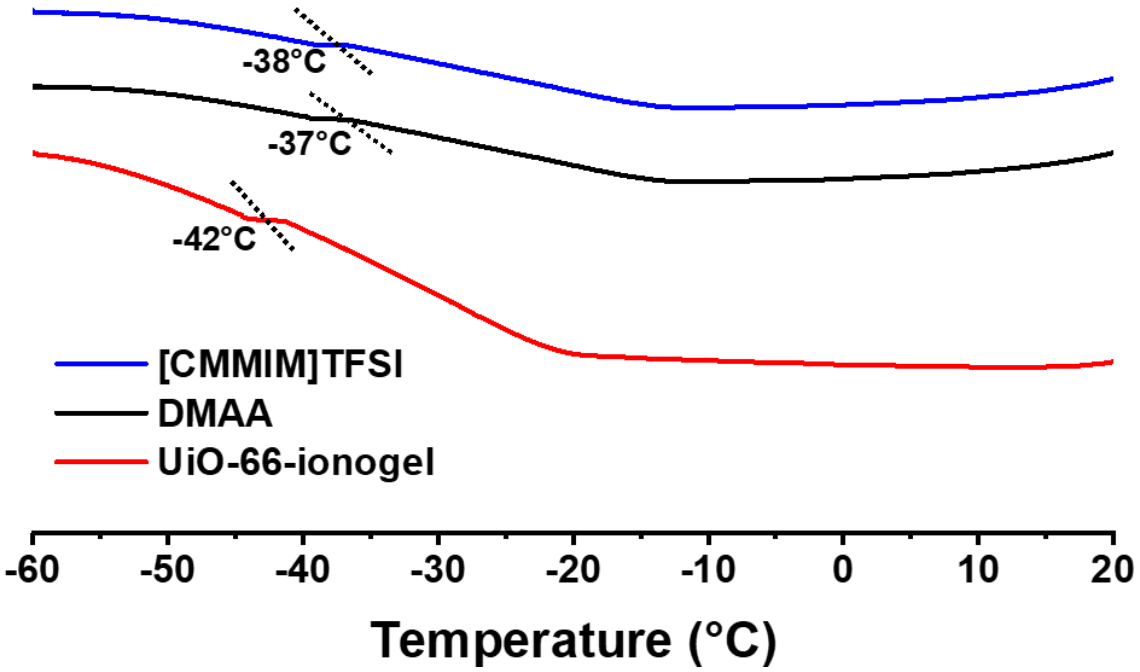

Figure S11. Dynamic scanning calorimetry (DSC) curves of ionic liquid [CMMIM]TFSI, DMAA, and UiO-66-ionogel between -60 and 20 ℃. The test was carried out at a scanning speed of 5 ℃ min^{-1} under N_2 condition.

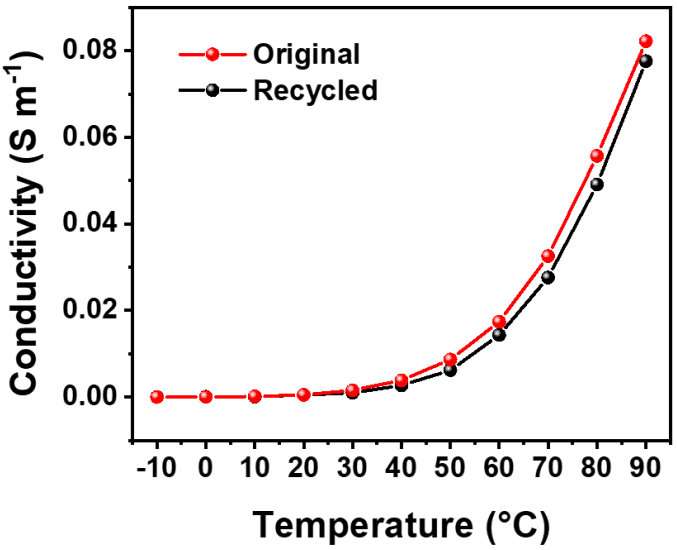

Figure S12. Conductivity of original and recycled UiO-66-ionogel (IL: 80 wt%, UiO-66: 0.5 wt%) at different temperatures. The graph showed that the conductivity increased with increasing temperature.

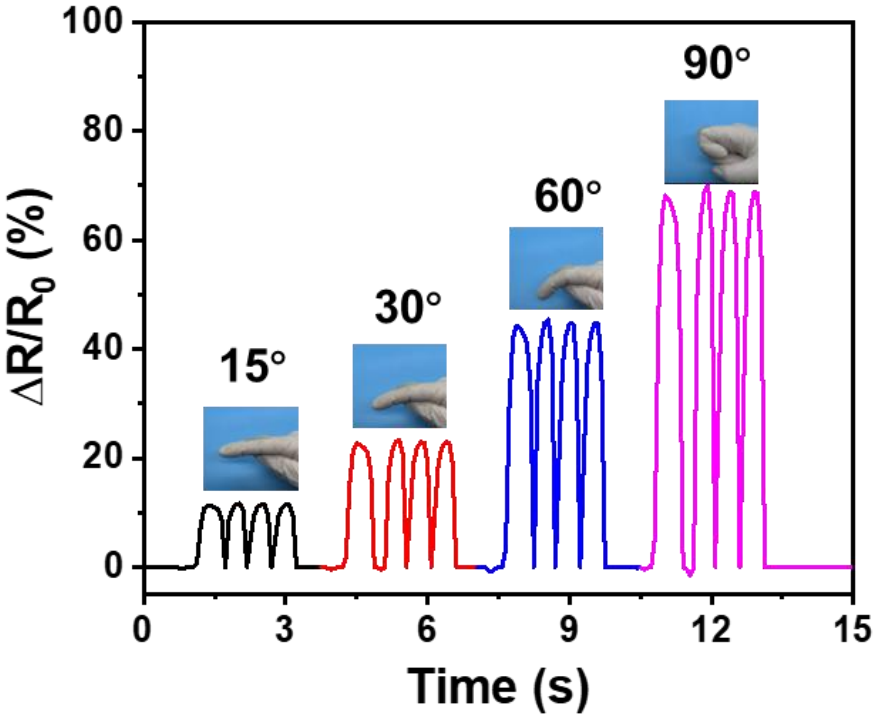

Figure S13. Signals of relative electrical resistance during finger bending.

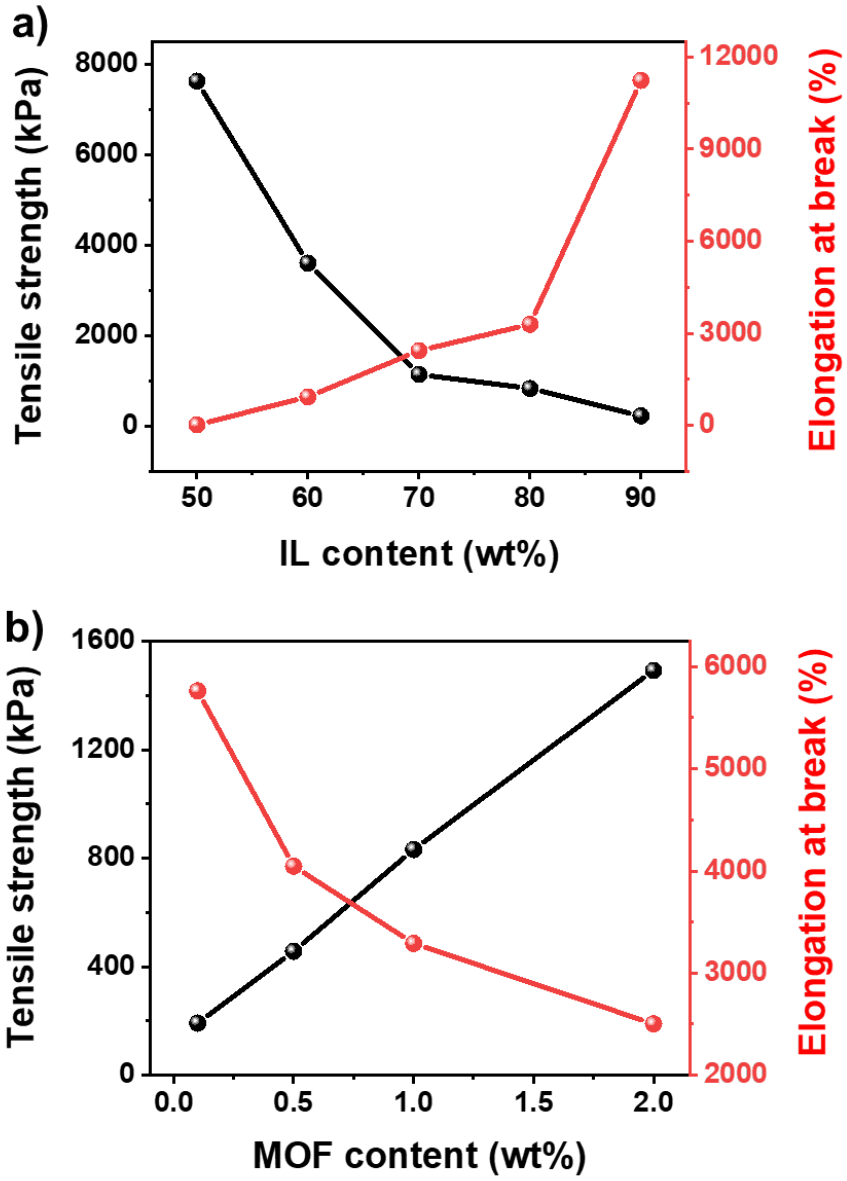

Figure S14. (a) Tensile strength and elongation at the break of UiO-66-ionogels with different IL contents at a UiO-66 content of 1.0 wt %. (b) Tensile strength and elongation at the break of UiO-66-ionogels with different MOF contents at IL content of 80 wt %.

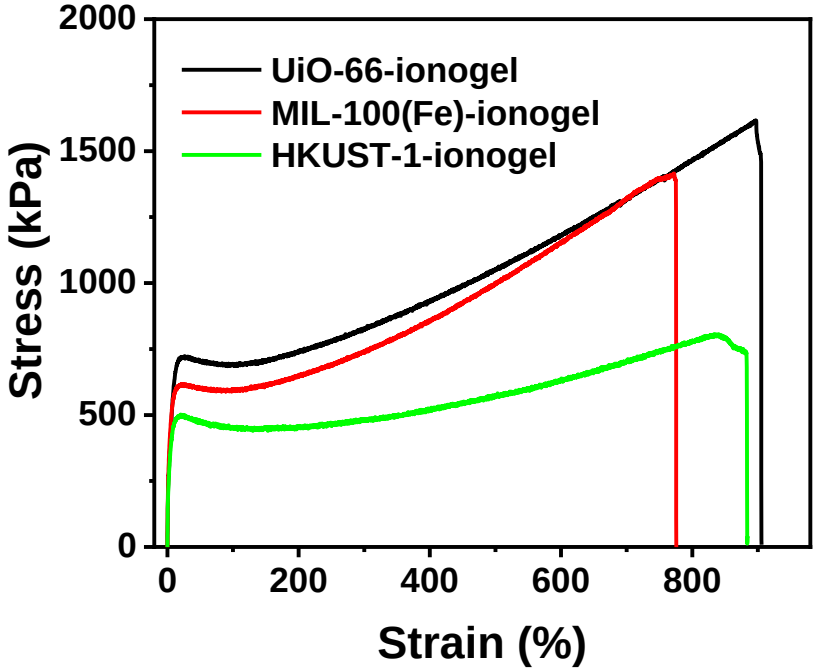

Figure S15. Tensile stress-strain curves of three MOFs (UiO-66, MIL-100(Fe), and HKUST-1) as crosslinking agents (IL:80 wt%, MOFs: 1.0 wt%). When UiO-66 was used as a crosslinking agent, the stress increase was the highest. The excellent mechanical properties confirm the applicability of the method.

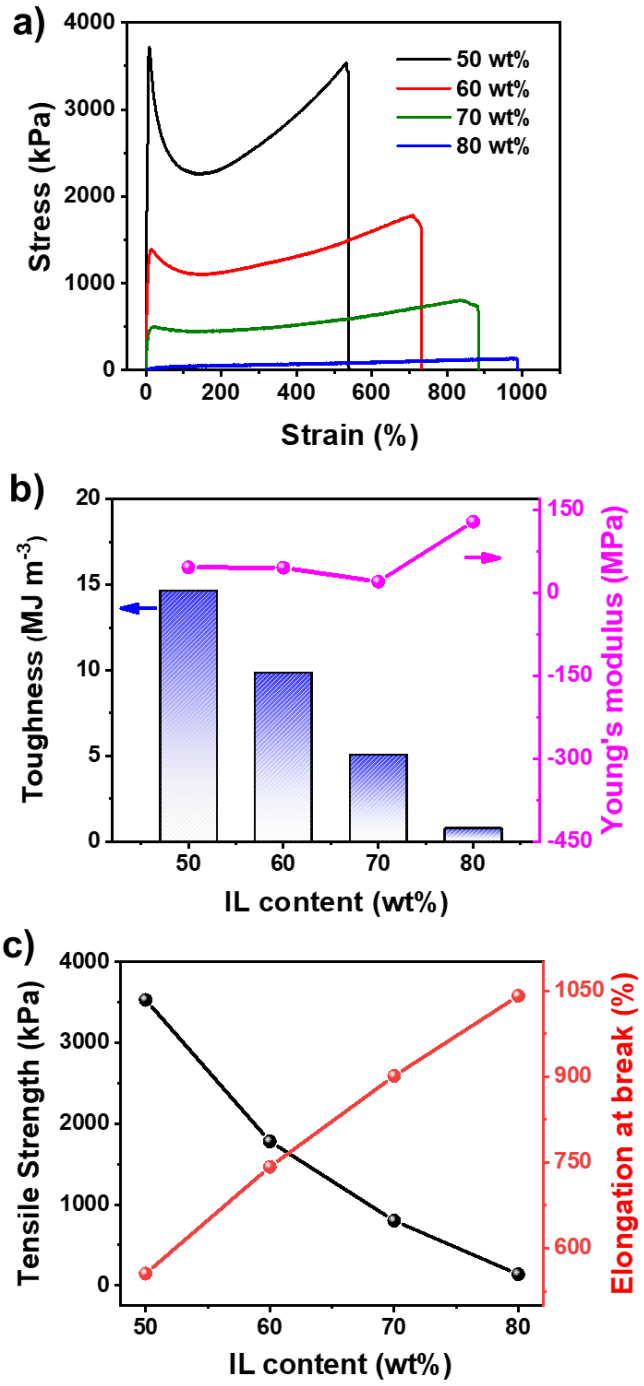

Figure S16. (a) Monotonic tensile stress-strain curves, (b) toughness and Young's modulus, and (c) tensile strength and elongation at break of HKUST-1-ionogels at different IL contents with 1.0 wt % HKUST-1.

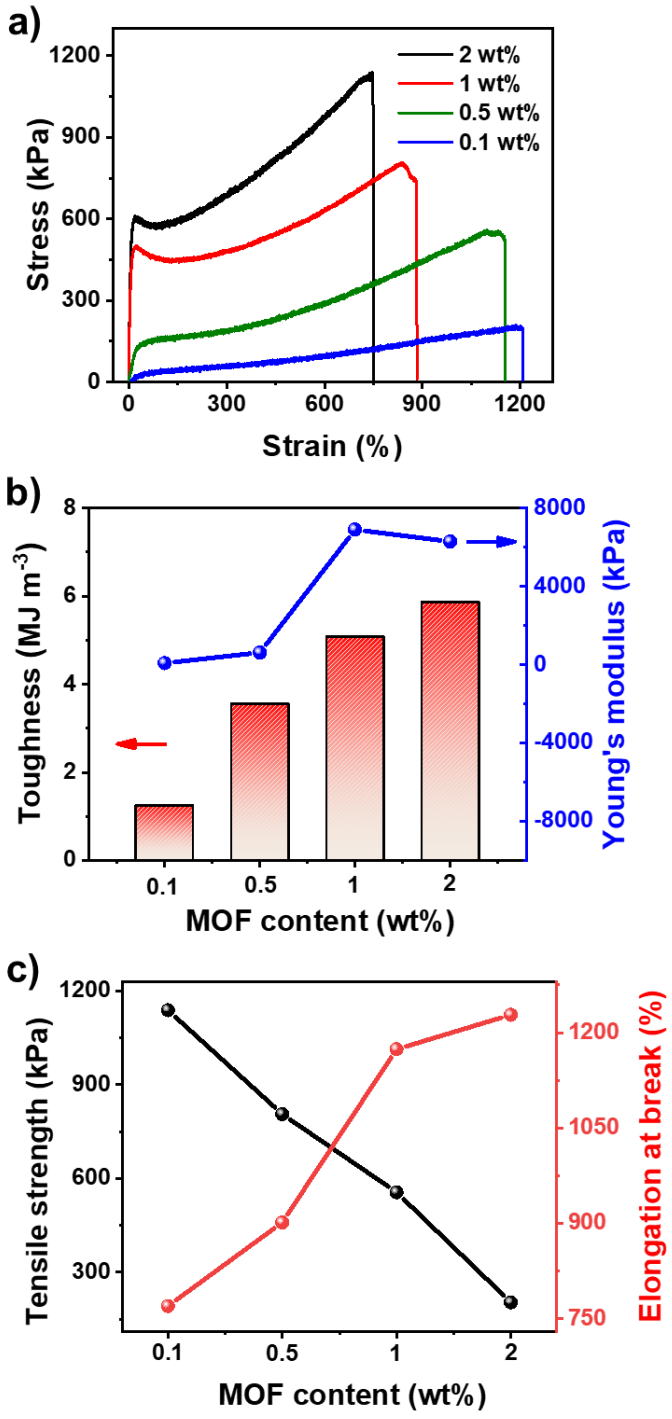

Figure S17. (a) Monotonic tensile stress-strain curves, (b) toughness and Young's modulus, and (c) tensile strength and elongation at break of HKUST-1-ionogels at different HKUST-1 contents with 80 wt % IL.

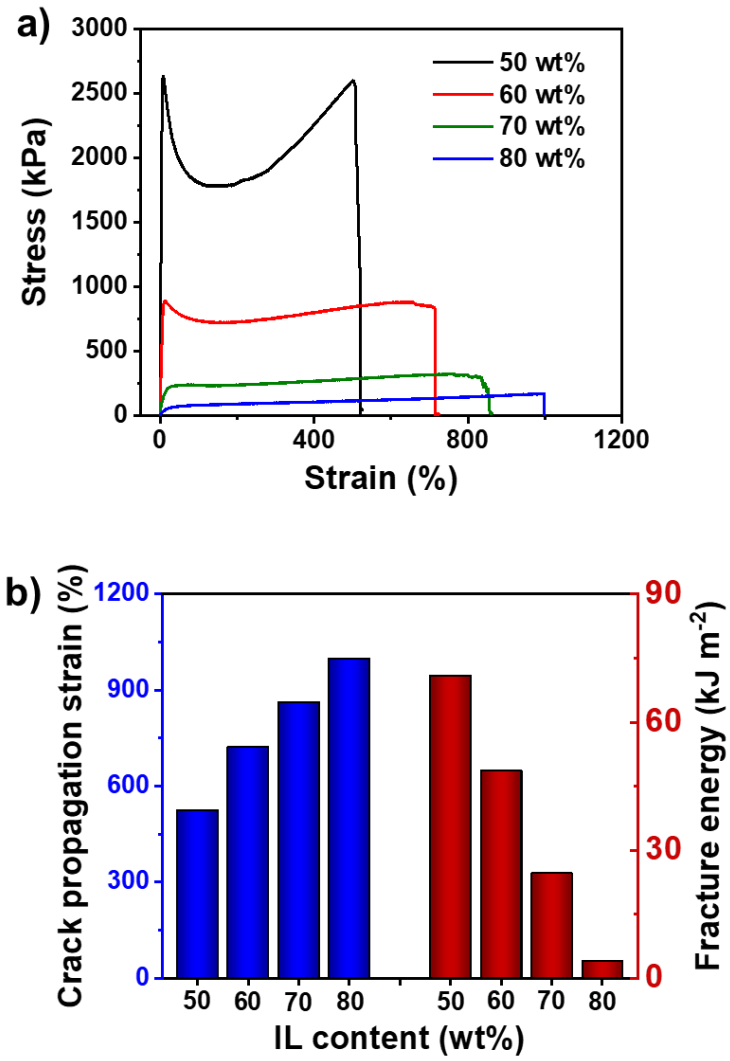

Figure S18. (a) Tear resistance of 1.0 wt% HKUST-1-ionogels with different ionic liquid contents. (b) Calculated crack propagation strain and fracture energy. HKUST-1 also prevents crack diffusion effectively.

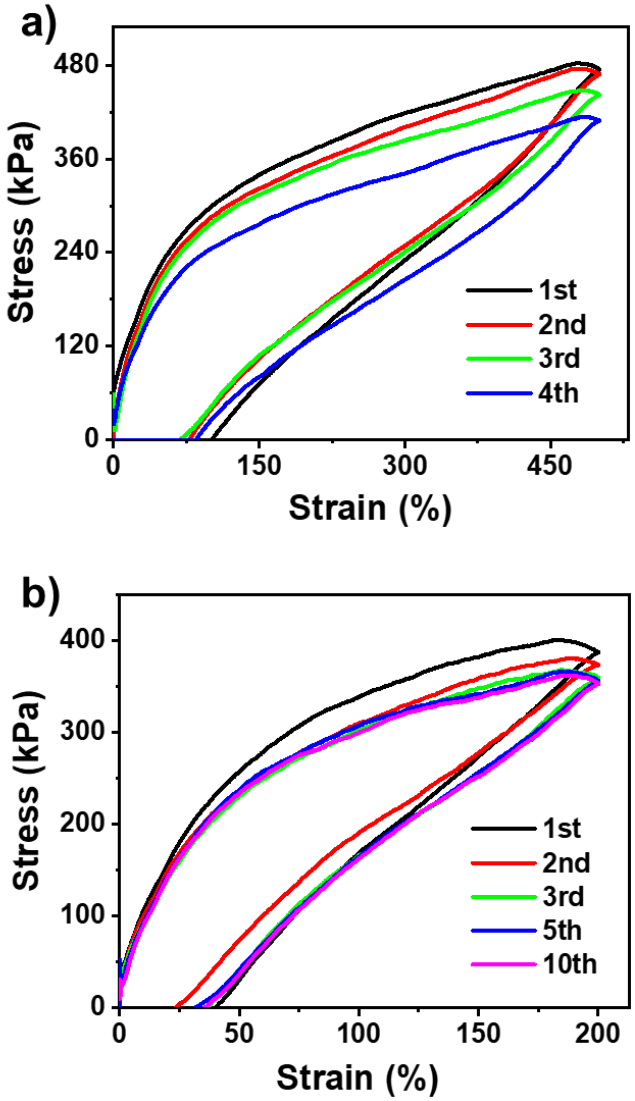

Figure S19. Cyclic stress-strain curves of HKUST-1-ionogels at (a) 500% and (b) 200% with 5 min intervals. The HKUST-1-ionogels were pre-stretched before the test.

Table S1. Comparison of the mechanical properties of the UiO-66-ionogels presented in this paper and representative gels in recent years.

	Stress (MPa)	Strain (%)	Young's modulus (MPa)	Fatigue threshold (kJ m^{-2})
This work	**7.6**	**11243**	**58**	**125**
Ref 16:*Nat. Mater.* 2022, *21*, 359	12.6	None	None	None
Ref 18:*Nano Energy.* 2021, *90*, 106645	5	600	None	None
Ref 47:*Adv. Mater.* 2021, *33*, e2105306	0.72	2066	None	None
Ref 48:*Adv. Funct. Mater.* 2021, *31*, 2102773	0.8	2580	0.102	2.35
Ref 49:*Adv. Mater.* 2021, *33*, 2006111	7	1640	0.9	None
Ref 50:*Adv. Funct. Mater.* 2021, *31*, 2102386	15.6	720	None	None
Ref 51:*J. Mater. Chem. A* 2022, *10*, 12005	7.42	1011	0.08	None
Ref 52:*Nat. Commun.* 2022, *13*, 2279	1.7	30000	18	95.265
Ref 53:*Chem. Mater.* 2021, *33*, 8418	0.15	450	0.06	0.45
Ref 54:*Adv. Mater.* 2015, *27*, 6990	6	2000	None	None
Ref 55:*Adv. Mater.* 2018, *30*, e1706846	1.5	1200	0.98	12
Ref 56:*Soft Matter.* 2014, *10*, 7993	0.18	2800	0.7	0.18
Ref 57:*Mater. Horizons* 2020, *7*, 912	1.7	5000	0.484	4.7
Ref 58:*Soft Matter.* 2014, *10*, 7519	1.1	2000	6.37	30
Ref 59: *J. Polym. Sci. Pol. Phys.* 2015, *53*, 1763	0.7	1300	None	6.8
Ref 60:*Adv. Funct. Mater.* 2015, *25*, 471-480	1	100	5.6	5.5
Ref 61:*Adv. Mater.* 2016, *28*, 40	0.002	200	0.0184	0.0396

References

[S1]. X. Peng; L. Ye; Y. Ding; L. Yi; C. Zhang; Z. Wen, Nanohybrid photocatalysts with ZnIn2S4 nanosheets encapsulated UiO-66 octahedral nanoparticles for visible-light-driven hydrogen generation. *Applied Catalysis B: Environmental,* **2020,** *260*, 118152.

[S2]. C. Yue; L. Wu; Y. Lin; Y. Lu; C. Shang; R. Ma; X. Zhang; X. Wang; W. D. Wu; X. D. Chen; Z. Wu, Study on the Stability, Evolution of Physicochemical Properties, and Postsynthesis of Metal–Organic Frameworks in Bubbled Aqueous Ozone Solution. *ACS Appli. Mater. Interfaces,* **2021,** *13*, 26264.

[S3]. M. Bagheri; A. Melillo; B. Ferrer; M. Y. Masoomi; H. Garcia, Improved catalytic hydrogen release of quasi HKUST-1 compared to HKUST-1. *Chem. Com.,* **2021,** *57*, 11964.